ELSEVIER

Polymer 42 (2001) 5247–5256

polymer

www.elsevier.nl/locate/polymer

Shear-induced crystallization of isotactic polypropylene with different molecular weight distributions: in situ small- and wide-angle X-ray scattering studies

A. Nogales[a,b], B.S. Hsiao[a,*], R.H. Somani[a], S. Srinivas[c], A.H. Tsou[c], F.J. Balta-Calleja[b], T.A. Ezquerra[b]

[a]*Department of Chemistry, State University of New York, Stony Brook, NY 11974-3400, USA*
[b]*Instituto de Estructura de la Materia, (C.S.I.C.), Serrano 119, Madrid 28006, Spain*
[c]*ExxonMobil Chemical Company, Baytown Polymers Center, Baytown, TX 77522, USA*

Received 2 August 2000; received in revised form 29 November 2000; accepted 1 December 2000

Abstract

In situ synchrotron wide-angle X-ray scattering (WAXS) and small-angle X-ray scattering (SAXS) were used to monitor the structural and morphological developments during crystallization of a series of isotactic polypropylene (iPP) blends with different molecular weight distributions (MWD). The experiments were carried out in the undercooled melt at 150°C subjected to a high shear strain (1428%) at a fixed shear rate (57 s^{-1}). The final WAXS patterns showed arcing of the main Bragg reflections, indicating the presence of oriented crystallites. These oriented crystallites, in the form of lamellae, were also revealed by two strong meridional reflections in the SAXS patterns. The crystallization kinetics exhibited a strong dependence on the molecular weight distribution, which were due to the production of primary nuclei induced by orientation. A method to deconvolute the total integrated scattered intensity (SAXS and WAXS) into the isotropic and anisotropic contributions from the crystallized polymer was used to analyze the data. The fraction of oriented morphology determined by SAXS and that of oriented crystallinity determined by WAXS showed good agreement with each other. However, it has been demonstrated that the oriented fraction from SAXS is more suitable for determining the 'critical orientation molecular weight' (M^*) value. Only polymer chains above M^* in the distribution can become oriented at a given shear rate. It is observed that, regardless of the MWD, a similar value for M^* is obtained under our experimental conditions.

Keywords: Isotactic polypropylene; Molecular weight distributions; Small- and wide-angle X-ray scattering

1. Introduction

Processing of polymeric materials involves the application of different levels of flow fields (elongation, shear, mixed) to the polymer melt [1]. These flow fields introduce different degrees of anisotropy to the polymer melt, which modify the nucleation and crystallization behavior. A great deal of effort has been devoted to elucidate the structure formation during crystallization, under elongational flow in polymer melts using flow injection molding methods [2–4]. Compared to elongational flow, shear flow is usually considered a weaker flow to provide extension of polymer chains.

During shear flow, the presence of connectivity between individual chains, in the form of chain entanglements is also sufficient to achieve chain extension, which then takes place between these topological constraints [5]. Under these circumstances, changes are produced in the resulting crystalline morphology, from spherulitic to crystallites oriented in the flow direction [6]. Among the variety of oriented structures that may occur when crystallizing from deformed melts, special attention has been given to shish–kebab structures. In these structures, extended chains in the direction of the applied strain act as row nuclei. Chain folded lamellae, oriented, to a first approximation, perpendicular to the extension axis, are produced by epitaxial nucleation on the surface of these row structures [5]. Also, it has been demonstrated, that shear flow accelerates, the overall crystallization kinetics, [7–14], due to an increase in the nucleation rate, caused by orientation of the polymer chains [15]. A strong effect of molecular weight and molecular weight distribution (MWD) has been observed in shear-induced crystallization. It was suggested that the high molecular weight species played an important role in melt orientation

* Corresponding author. Tel.: +1-631-632-7793; fax: +1-631-632-6518.
E-mail address: bhsiao@notes.cc.sunysb.edu (B.S. Hsiao).

0032-3861/01/$ - see front matter
PII: S0032-3861(00)00919-8

Table 1
Molecular weights and MWD of the iPP resins

Sample designation	A (%)	$M_n \times 10^4$ (g/mol)	$M_w \times 10^5$ (g/mol)	M_w/M_n	T_m (°C)
I	0	3.19	1.48	4.65	165
I/A 96/04	4	3.21	1.54	4.81	165
I/A 92/08	8	5.94	1.59	2.68	165
I/A 84/16	16	3.32	1.78	5.36	165
A	100	4.37	3.09	7.08	165

and enhancement in crystallization kinetics [16,17]. A summary of shear-induced crystallization studies has been compiled by Tribout [18].

The structure of isotactic polypropylene (iPP) reflects very sensitively the changes in processing parameters such as thermal conditions, applied shear (or elongation) rate, strain, and duration [19]. Also, its crystallization behavior is strongly dependent on molecular parameters such as molecular weight, MWD and chain branching. Several studies of the effects of shear (and elongation) fields on the crystalline morphology of iPP have been carried out. For example Varga [20] studied shear-induced crystallization of iPP and copolymers using a thermo-optical technique. They concluded that melt-shearing caused the development of row nuclei in the form of microfibrillar bundles. Row-nuclei generated the epitaxial growth of folded chain lamellae perpendicular to the row-nuclei, resulting in a supramolecular structure of cylindrical symmetry. The latter form was referred to as a cylindrite by Kargin [21], and Binsenbergen [22]. Kornfield and coworkers [23] investigated the effects of short term shearing on the subsequent crystallization of a polydisperse iPP using in situ optical and wide-angle X-ray diffraction (WAXD) measurements, and ex situ microscopy. Ex situ optical and electron microscopy [24] of the polypropylene specimens quenched after shear crystallization revealed highly oriented crystallites developed in a row nucleated or shish–kebab morphology; the parent lamellae (kebabs) grew radially from the central line nuclei (shish) until they impinged with each other.

Misra [25] studied the role of molecular weight distribution on the spinnability, structure, and properties of melt-spun iPP fibers. Vleeshouwers and Meijer [17] reported the influence of shear on isothermal crystallization of iPP of different molecular weights and MWD. Shear rate and time revealed independent effects on crystallization. Short times at high rates were found to be most effective in accelerating crystallization kinetics. Furthermore, it was shown that the crystallization behavior was very sensitive to molecular weight and MWD. Moitzi and Skalicky [26] indicated that even a small shearing of melt, for a few seconds, enhanced the crystallization of iPP between 130 and 135°C. In a recent study [27], Haudin and Monasse, measured the crystallization kinetics of polypropylenes with various molecular weights during shear in a fiber-pullout device. They observed that the sensitivity of a given polypropylene to shear depended on its molecular weight. Eder and coworkers have further shown that the dependence of the rheological properties of molten linear polymers on the high molecular weight tail of the MWD was critical [28].

We have recently reported in situ synchrotron small-angle X-ray scattering (SAXS) experiments during isothermal crystallization of iPP at 140°C after step-shear deformation [29]. The SAXS patterns showed strong scattering maxima in the meridian immediately after cessation of shear, due to the rapid development of oriented polymer lamellae (kebab-like) within the melt. We have shown that the oriented fraction in the polymer bulk depends on shear rate, being lower for the lowest shear rate applied. Furthermore, we found that only the polymer molecules above a "critical orientation molecular weight" (M^*) in the distribution become oriented at a given shear rate. Analysis of results suggest that the value of M^* is more sensitive at low shear rates and remains about constant at high shear rates.

The aim of the present study is to investigate, more in detail, the role of the high molecular weight species on crystallization after step-shear. To achieve the goal of having different concentrations of high molecular weight species, blends of two iPP resins with very different molecular weights were studied. In situ small- and wide-angle X-ray scattering were performed in order to study the development of crystallization and morphology induced by shear.

2. Experimental

2.1. Materials

A series of Ziegler-Natta iPP homopolymers and blends, provided by ExxonMobil Chemical Company, were used. The blends contained two different molecular weight materials: one iPP homopolymer of lower molecular weight, designated as resin I; second homopolymer of higher molecular weight, designated as resin A. Further details of the molecular composition of the blends from GPC data are given in Table 1. Polymer blends were prepared by melt extrusion. The selected blend compositions used in this study are shown in Table 1. The melting temperatures of the blends were determined by DSC, and are also shown also in Table 1.

Polymer films of 0.5–1.0 mm thickness were prepared by

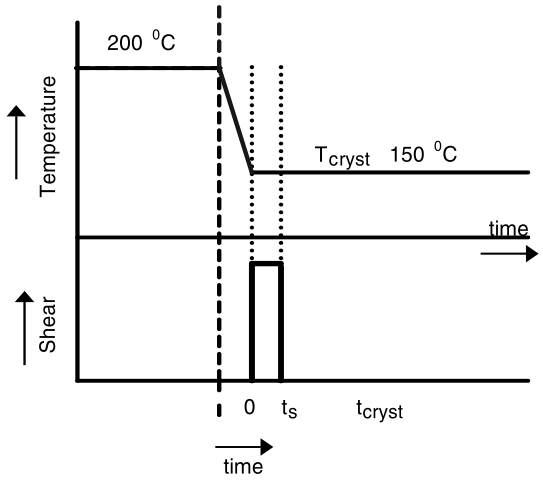

Fig. 1. Schematics diagram of temperature profile followed in the step shear experiments.

compression molding at 200°C. Samples in the form of a ring (ID = 10 mm, OD = 20 mm) were cut from the molded films for X-ray measurements.

2.2. Instrumentation

A Linkam CSS-450 high temperature optical shearing stage modified for in situ X-ray scattering studies was used to apply a controlled shear-field and thermal history to the polymer sample. Kapton X-ray windows were used in place of the standard quartz optical windows on the top and bottom steel blocks of the Linkam stage. The top window had a narrow aperture hole, which allowed the X-ray beam to enter the sample. The bottom window, which was also the rotating window, had three open slots (wider than the hole in the top window). This design is similar to the one published by Burghardt and coworkers [30]. The sample was held in the gap between the two windows. The sample was completely enclosed in the cell. As the polymer melts were fairly viscous, no leakage was detected even when the Linkam stage was mounted in the vertical position.

The mechanical design and electronics of the Linkam stage provided precise control over the various parameters of the shear experiment; such as temperature, heating/cooling rates, gap, shear strain, rate, and duration, as well as the shear mode such as, step, steady, and oscillatory. In all our experiments, the duration of the step shear impulse was 0.25 s (shear rate $\dot{\gamma}$ equal to 57 s^{-1}). A high strain value of 1428% was used in all our experiments.

Wide-angle X-ray scattering (WAXS) measurements were carried out at the SUNY Beamline (X3A2, $\lambda = 1.54$ Å) in the National Synchrotron Light Source (NSLS), Brookhaven National Laboratory (BNL). The shear stage was placed perpendicular to the incident X-ray beam. The aperture hole in the top window of the shear stage was aligned with the incident X-ray beam. Two-dimensional scattering patterns were obtained by means of a MAR CCD X-ray detector. The detector was placed at a distance of 140 mm from the sample. Corresponding small-angle X-ray scattering (SAXS) measurements were carried out separately at the Advanced Polymers Beamline (X27C, $\lambda = 1.307$ Å) in NSLS, BNL. The detector was placed at a distance of 1700 mm from the sample. The maximum resolution of the SAXS set-up is about 1000 Å.

2.3. Procedure

In each experiment, the polymer sample was mounted between the two X-ray windows. The gap between the two windows was set equal to the sample thickness. In order to ensure that the polymer melt is free of any memory effects associated with clusters or crystal aggregates due to the prior temperature, deformation or crystallization history, all polymer samples were subjected to the following thermal history, as shown in Fig. 1. The samples were heated to 200°C (substantially above the nominal melting point of the isotactic polypropylene resin ~165°C) and held for 5 min. Both the SAXS and WAXD patterns taken at 200°C showed only a diffuse ring (halo) from the amorphous melt and did not show any indications of residual crystal clusters or aggregates. The melt was cooled at 30°C/min and SAXS and WAXD patterns were collected before the application of shear; the X-ray patterns showed only a diffuse ring from the amorphous melt, similar to that observed at 200°C.

The chosen crystallization temperature (150°C) was high enough to ensure that the crystallization times were sufficiently long (crystallization times longer than 10^4s) under quiescent conditions. Two-dimensional X-ray images (SAXS and WAXD) were recorded as soon as the polymer reached the measurement temperature (150°C). The data acquisition time for each scattering pattern (image) was 20 s, with a pause time of 5 s between adjacent images. The program was set for collecting 80 consecutive images. The scattering images were collected continuously; before, during, and after cessation of the applied shear. It should be noted that the scattering images represent the average of the scattered intensity from the scatterers across the thickness of the sample.

An air scattering pattern (also collected at 20 s acquisition time) at the measurement temperature was collected with no sample between the two windows of the shear stage. The air scattering pattern was used for the background correction of the scattering images of the polypropylene samples. X-ray data were also normalized for sample thickness. Subsequent analysis of the X-ray data was carried out on the corrected and normalized scattering patterns.

3. Data analysis

3.1. WAXS

The two-dimensional WAXS patterns were corrected, in the first step, for the incident beam intensity fluctuations.

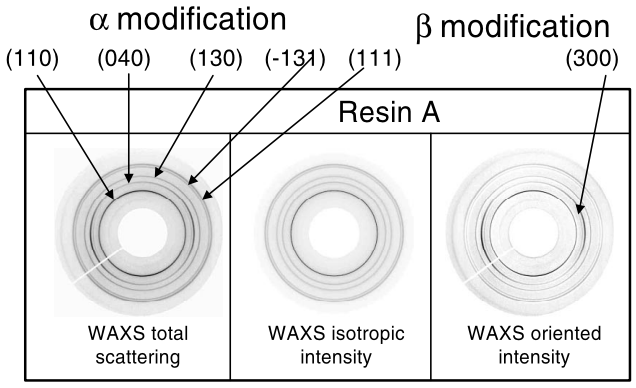

Fig. 2. Example of analysis of the WAXS patterns (700 s after cessation of the shear field). Total scattered intensity (left), calculated isotropic scattered intensity (center) and oriented scattered intensity (right) from resin A.

Also air scattering, obtained at T_c, was subtracted from all the patterns. To analyze the WAXS patterns, the first step is to separate the contributions to the total intensity from the oriented and unoriented scatterers. Here, we assume that the morphology consists of two parts, an oriented part and an isotropic part. As discussed in detail later, we speculate that the high molecular weight species (with long relaxation times) in the distribution are primarily responsible for the formation of shear-induced nuclei. These nuclei provide sites for growth of the oriented lamellae. The relaxed polymer melt takes part in the growth of both the oriented and unoriented crystals. It is understood that an entire distribution of crystal orientation (extent or degree of orientation) exists; however, the total scattered intensity is separated into only two contributions. One, the isotropic contribution from the amorphous chains and the unoriented crystals, and second, the oriented contribution from all oriented (with varying degree of orientation) scatterers. To estimate the different contributions from the respective species, we assume that the azimuthally independent component of the total scattered intensity is directly proportional to the unoriented fraction of the material. Based on this assumption, we can calculate the oriented fraction of the polymer from the integrated scattered intensity values by subtracting the azimuthally independent component from the total scattered intensity. To determine the azimuthally independent intensity, we used a method previously developed in this laboratory [31]. For each 2θ angle, the minimum value of the intensity across the azimuthal scan can be considered as from the envelope intensity of the unoriented species. By recording all the minimum values for each 2θ value, the isotropic contribution can be generated (note that the minimum values due to noise or detector defects can be corrected by data extrapolation). This isotropic contribution is subtracted from the two-dimensional WAXS scattering pattern, yielding the oriented contribution. This method is exemplified in Fig. 2 for the case of the two-dimensional WAXS pattern of resin A obtained 1475 s after cessation of shear. Using this method, one can extract the fraction of oriented crystals (oriented crystallinity), as

$$X_c^{or} = \frac{\text{Oriented scattering}}{\text{Total scattering}} \tag{1}$$

As mentioned above, the unoriented scattering contains two contributions. The first one comes from the scattering of the amorphous chains; the second one originates from the isotropically oriented crystals. To separate these two contributions, linear profiles were obtained from the unoriented contribution. A peak-fit procedure was then used to calculate the crystalline percentage of the unoriented crystal fraction. The shape of the amorphous contribution was obtained from the isotropic images of the quiescent polymer melt (the first image before shear). The shape of the amorphous profile was kept constant, with variable intensity. Gaussian functions were used to fit the crystalline reflections, and their peak parameters were iterated to achieve a good fit with the experimental data. An example of this kind of peak separation is illustrated in Fig. 3. The contribution of the randomly distributed crystals to the scattering patterns can be calculated from the area underneath the crystalline peaks.

After this analysis, it is then possible to obtain the fraction of randomly distributed crystals (unoriented crystallinity), as

$$X_c^{unor} = \frac{\text{Unoriented crystalline scattering}}{\text{Total scattering}} \tag{2}$$

The mass fraction of the amorphous chains thus become

$$X_A = 1 - X_c^{or} - X_c^{unor} \tag{3}$$

Such an approach implicitly assumes that there is little or no amorphous phase contribution to the oriented scattering, which is confirmed by calculating the degree of crystallinity from the oriented scattering.

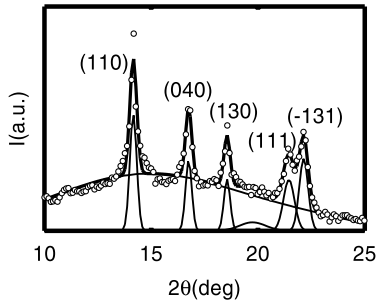

Fig. 3. Peak deconvolution analysis to separate the crystal reflections and amorphous background scattering from the unoriented WAXS profile.

3.2. SAXS

For the SAXS data treatment, a procedure similar to the one used for the WAXS data was employed. The total SAXS integrated intensity from the polymer sample, again, can be separated into two components: one arising from the randomly distributed scatterers in the sample (isotropic contribution), and the other originated by the oriented

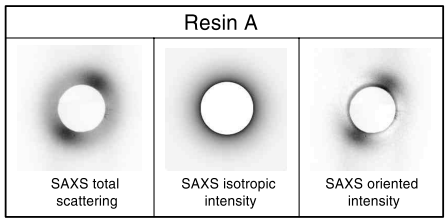

Fig. 4. Analysis of the SAXS patterns (885 s after the cessation of the shear field). Total scattered intensity (left), calculated isotropic scattered intensity (center) and oriented scattered intensity (right) from resin A.

species (anisotropic contribution). The isotropic contribution (Φ_{iso}) is azimuthally independent, while the scattering arising from the oriented species (Φ_{or}) is azimuthal dependent. An example of application of this method to SAXS data is shown in Fig. 4 for the case of the two-dimensional SAXS pattern obtained 1200 s after cessation of shear for resin A. The physical implications of these fraction determined by SAXS and WAXS are different as explained later in the paper.

4. Results

4.1. WAXS

Fig. 5 shows representative two-dimensional WAXS patterns obtained after cessation of step shear ($\dot{\gamma} = 57\ s^{-1}$) for the two homopolymers (I and A) and for the blend I/A (92/08). The initial X-ray scattering patterns for the three samples show diffuse rings representing scattering from an isotropic melt. These diffuse rings, obtained after cessation of shear, do not show any orientation. As crystallization proceeds, discrete reflections appear over the diffuse halo. These reflections can be indexed as the (110), (040), (130), (111) and (−131) of the α-monoclinic form of iPP [32,33]. There is evidence of a reflection at the equator around $2\theta = 16°$ indicating the presence of β-phase in all the samples (as also shown in Fig. 2). The amount of the β-phase appears to increase with shear rate. We will discuss this behavior in detail later in another paper.

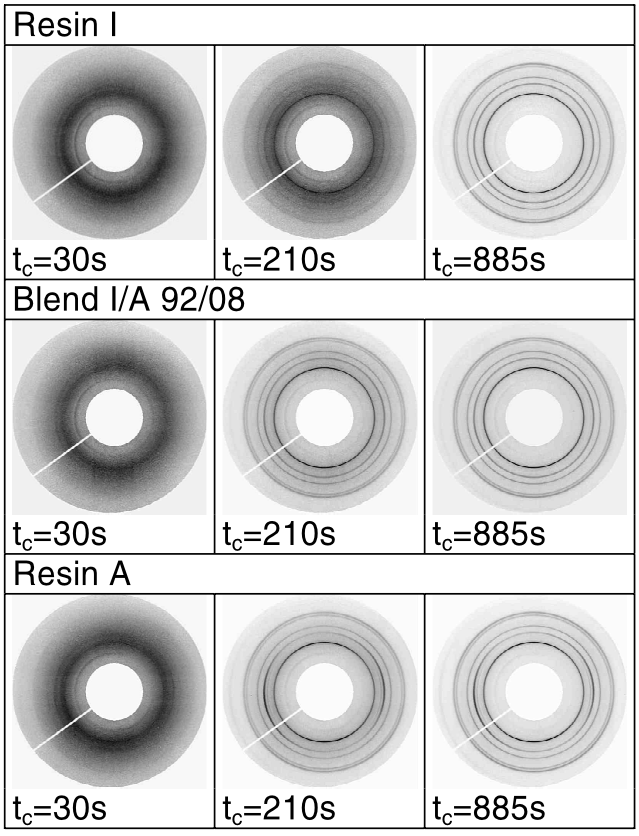

Fig. 5. Selected two dimensional WAXS patterns obtained after cessation of the step shear ($\dot{\gamma} = 57\ s^{-1}$) for the three studied iPP samples.

There are some features worth mentioning concerning the evolution of the scattering images, which appears to be a function of the molecular weight composition of the sample. First of all, one sees that, the kinetics of the Bragg ring's evolution is slower for resin I, (low molecular weight sample) than for the blend I/A 92/08 and for resin A (higher Mw). Another relevant difference is based on the azimuthal intensity distribution of the Bragg rings. In case of resin A, the initial crystalline rings are clearly concentrated around the principal experimental axes, the flow direction is nearly vertical indicating that the initially developed crystals are highly oriented. As crystallization time increases, these rings become more intense but less oriented, indicating that the crystals developing in the later stages of crystallization are randomly oriented. This effect though cannot be clearly identified for resin I and blend I/A 92/08 by visual-inspection of Fig. 5, it is nevertheless present, to a lesser extent in these samples, as will be discussed in the following sections.

4.2. Azimuthal analysis of the WAXS patterns

The azimuthal orientation distribution of the WAXS reflections indicates that, all the samples studied exhibit some degrees of orientation when crystallized for 1200 s after shearing. The crystalline orientation is revealed by arcing in the meridional, innermost (110) reflection (see for example Fig. 2, flow direction is vertical). The next reflection, (040), is most intense in the equator. The variation of these two reflections with azimuthal angle for resin A is presented in Fig. 6. As is known, the *hk0* reflections represent lattice planes parallel to the *c*-chain axis, which in our experiments coincides with the flow direction. Consequently, the (040) intensity distribution along the equator indicates the expected crystallite orientation in the flow direction. The arcing on the meridional (110) has been discussed by Padden et al. [34] and Lotz et al. [35]. These authors described the occurrence of the meridional reflection in terms of epitaxy on the lateral *ac*-faces of the α-phase, causing lamellar branching of crystallites in the daughter lamella with

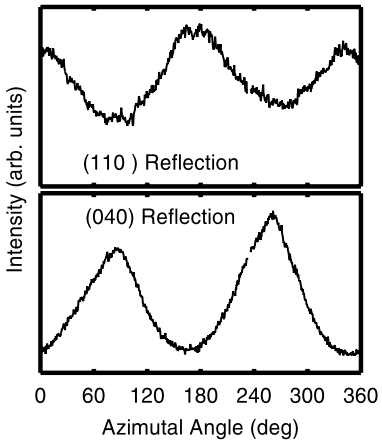

Fig. 6. Azimuthal trace of iPP (110) and (040) reflections from the corrected WAXS pattern of Fig. 2 (resin A, 885 s after crystallization).

their a^*-axis (originated by a-axis of the daughter lamella) in the flow direction [36].

The sample composition affects the variation of the reflection intensities with the azimuthal angle. Fig. 7 illustrates the variation of the equatorial (040) reflection as a function of the azimuthal angle for the different samples studied. It is evident that as the high molecular weight polymer concentration in the blend is increased, the azimuthal variation of the reflection becomes more conspicuous, implying higher degree of orientation.

4.3. Dependence of crystallinity on blend concentration

The evolution of the total crystallinity, X_c, the crystallinity of oriented scatterers X_c^{or}, and the randomly distributed (unoriented) scatterers, X_c^{unor}, at $T_c = 150°C$ are presented in Fig. 8 as a function of crystallization time t_c for all the samples studied. The overall crystallinity X_c (Fig. 8a), which includes both, the oriented and the randomly distributed crystals, increases in a different fashion for the two homopolymers (filled symbols). The lower molecular weight polymer (resin I) presents a slower kinetics than the higher molecular weight polymer (resin A). However, the maximum level of overall crystallinity

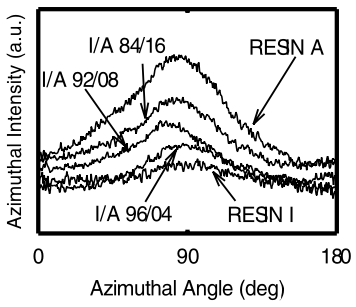

Fig. 7. Variation of the azimuthal intensities of the (040) reflection with blend concentration blend. From bottom to top, resin I, blend I/A 92/08, blend 84/16 and resin A.

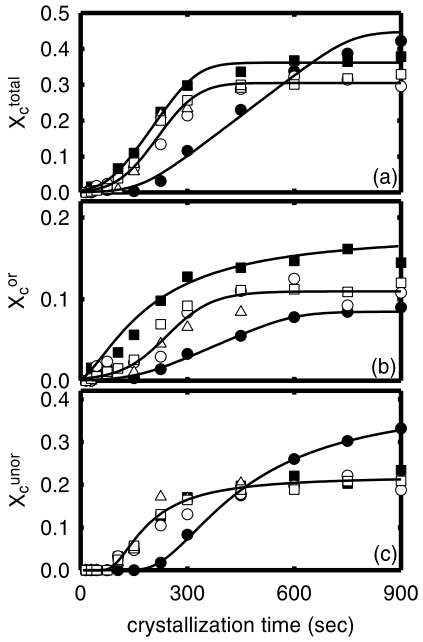

Fig. 8. (a) Total, (b) oriented, and (c) randomly distributed crystallinity for all the samples studied in this work. (●), resin I; (○), blend I/A 96/04; (□), blend I/A 92/08; (△), blend I/A 84/16; and (■), resin A.

reached by resin I is around 45%, whereas resin A reaches a maximum value of crystallinity of around 35%. Interestingly, the crystallization kinetics of all the blends are almost identical, regardless of the blend composition, and is very similar to the one exhibited by resin A (high molecular weight resin), presenting only differences in the final crystallinity level reached. Fig. 8b shows the evolution of the WAXS oriented crystallinity with t_c. Here one observes again, that there is a difference in the crystallinity increase for the two homopolymers with different molecular weights. A notable difference in the final oriented crystallinity for

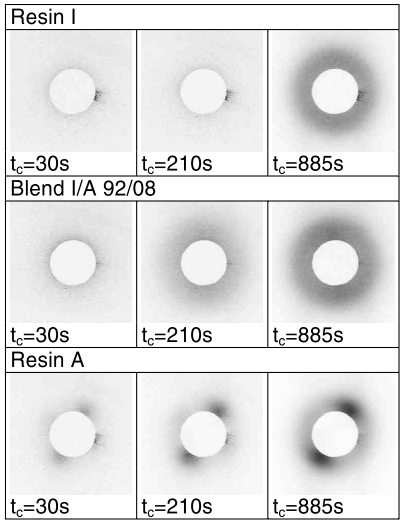

Fig. 9. Two dimensional SAXS patterns obtained after cessation of the step shear (57 s^{-1} shear rate) for three selected samples.

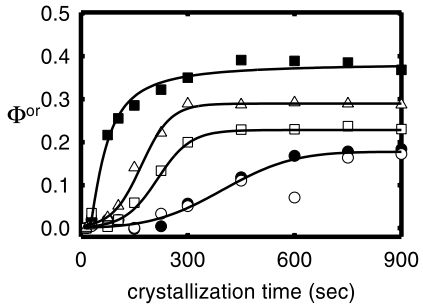

Fig. 10. Oriented fraction obtained from SAXS for all samples studied. (●), resin I; (○), blend I/A 96/04; (□), blend I/A 92/08; (△), blend I/A 84/16; and (■), resin A.

both resin A and I is also obtained. The lower molecular weight polymer (resin I) reaches about 8% of oriented crystallinity when crystallized at 150°C and for 1200 s after shearing. For the higher molecular weight polymer (resin A) the final level of oriented crystallinity is higher (around 15%). The blends, again exhibit kinetics, which resembles the one of resin A, though the final value of the oriented crystallinity is slightly smaller (around 10%).

Finally, the kinetics of the crystallinity increase from the randomly distributed crystals (Fig. 8c) presents similar features as those observed by the two previous crystallinity contributions, i.e. a slower kinetics for resin I than for resin A. However, it is worth noting the evolution of the random crystallinity with time. The blends exhibit exactly the same behavior as the higher molecular weight homopolymer (resin A). In this case, the amount of randomly distributed crystals is higher for the lower molecular weight sample (resin I) than for resin A. The final values of unoriented crystallinity exhibit, an opposite trend to the one observed for the oriented contribution.

4.4. SAXS

Fig. 9 shows representative two-dimensional SAXS patterns obtained for the three samples after cessation of step shear ($\dot{\gamma} = 57\ s^{-1}$). Similar to the case of the WAXS patterns, different molecular weight compositions display different features that are worth mentioning. For resin I, the initial image consists of a weak and almost negligible diffuse ring from the isotropic melt, indicating the absence of any detectable structure and preferred orientation. As crystallization proceeds, a circular reflection appears, corresponding to the development of a long spacing from the almost random lamellar structures. Only a very small orientation in the form of weak meridional maxima superimposed on the isotropic scattering ring can be detected. A similar situation is seen in resin I/A 92/08, though the ring pattern appears in this case earlier than for resin I. In addition, the two meridional maxima due to the presence of oriented lamellar structures are more enhanced than in case of resin I. On the other hand, the SAXS patterns shown by resin A are very different from the previous ones. Even for very short crystallization times, the patterns clearly show the appearance of meridional maxima arising from the oriented scatterers. As crystallization develops, these meridional maxima become stronger, and an additional weaker isotropic scattering ring corresponding to unoriented lamellar structures appears. A summary of the above mentioned features is presented and discussed in the next section.

4.5. Dependence of the SAXS oriented fraction with blend composition

From the SAXS experiment, it is also possible to separate the contribution of the anisotropic scattering from the total scattering. Fig. 10 shows the evolution of this SAXS oriented fraction for all the blends at an isothermal crystallization temperature of $T_c = 150°C$ after shear. In Fig. 10, one can observe that, as in the WAXS results, there is a significant difference between the crystallization behavior of resins I and A. The development of the oriented morphology in resin A (high molecular weight) is much faster that the kinetics of resin I. The amount of material that is finally oriented, from SAXS measurements, is lower in the case of the lower molecular weight material (only about 14% of material is finally oriented). The higher molecular weight iPP, resin A, reaches a value of around 35% for the oriented fraction. In the SAXS case, the dependence of the oriented fraction with the blend content appears to follow a simple rule of mixing. The behavior for the blend with lowest A content is similar to that of resin I. However, as the resin A content is increased, the kinetics becomes faster and the final fraction of the oriented morphology becomes higher. This situation is at variance with the WAXS results, where, as pointed out above, the behavior of the blends was the same regardless of their composition. The total integrated intensities from SAXS and WAXS were also very different. As WAXS registered a large contribution from the amorphous melt in the beginning, SAXS detected almost no scattered intensity from the homogeneous melt. The increase in the total WAXS intensity during crystallization is relatively small, as some contributions of the crystal phase are converted from those of the amorphous phase. In contrast, the increase in the total SAXS intensity during crystallization is very distinct.

5. Discussion

5.1. Crystallization kinetics

The WAXS and SAXS results in Figs. 8 and 10, respectively, show that the amount of the final oriented crystallinity (X_c^{unor}) detected by WAXS is smaller for all the samples than the oriented fraction detected by SAXS (Φ^{or}). It is quite obvious that the mass fractions values (X) calculated from WAXS are different from the scattering

fractions (Φ) calculated by SAXS. The X values are related to the crystallinity (oriented and unoriented) arising from the three dimensional ordered structures, while the values of Φ come from the product of the volume fractions of the crystalline and amorphous phases (Φ_c, Φ_a), and the scattering contrast due to the electron density difference $(\rho_c-\rho_a)^2$. In Figs. 8 and 10 one observes that, while X^{or} and X^{unor} exhibit the same trend for all the blends, regardless of the high molecular weight polymer concentration, the oriented fractions (Φ^{or}) estimated by SAXS exhibit notable differences depending on blend concentration. Recently, we have shown [37], by simulating different degrees of crystallinity in polymers, the WAXS detection limit for structures is smaller than that of SAXS. This may also attribute, at least in part, to the different trend in the orientated fraction of materials observed in WAXS and SAXS, respectively.

The crystallization kinetics, as determined by SAXS and WAXS are shown to be consistent with each other. By using both techniques, it is seen that, the homopolymer with higher molecular weight crystallizes faster than the lower molecular weight homopolymer. Under quiescent conditions, over a wide range of temperatures, the lower molecular weight materials crystallize faster [38] owing to the higher crystal growth rate (higher molecular mobility). In the present study it is assumed that the effect of growth rate does not play a role in the different kinetics observed. Instead it is believed that the increase in crystallization rate is mainly due to the increase in primary nuclei induced by flow. As the entropy of macromolecules in the random phase is near maximum (random coil conformation), shear deformation will induce an extension of the chains and consequently decrease the overall entropy. This process can, generate nuclei through a homogeneous nucleation process consisting of aggregates of oriented chains, which can greatly accelerate the crystallization kinetics.

5.2. Orientation versus relaxation

In our preceding paper [29], it was shown that, at a given shear rate, only the molecules with molecular weights higher than a 'critical orientation molecular weight' (M^*) could become oriented. For flow-induced crystallization, a certain degree of molecular extension (orientation) must be achieved. The motion of polymer chains due to an applied deformation field is governed by several factors, such as entanglement density, friction coefficient (due to local interactions between chain segments), chain stiffness, relaxation time, etc. It should be emphasized that the entanglements and disentanglements (which affect zero shear viscosity) are less of a concern than the relaxation behavior. Under isothermal conditions, the molecular weight is expected to play a major role in governing the extent of orientation and stability of the oriented structures after cessation of shear. Longer chain molecules take a longer time to relax after deformation than shorter ones, and thus, have a better chance of being oriented. In polymers with broad molecular weight distributions (chain lengths), the longer chains from the high molecular weight tail would give rise to orientation-induced nuclei due to higher orientation compared to the shorter chains. The short chain molecules relax in a very short time after deformation and hence cannot form nuclei under flow. The extent of orientation of the polymer molecules, and the stability of the resulting orientation-induced nuclei, depend on both the level of the deformation (strain) and on the deformation rate (shear rate or elongation rate) relative to the relaxation rate of the molecules. For flow induced crystallization, a certain degree of molecular extension must be achieved. When the time scale of straining is long relative to the time scale of disentanglement, orientation relaxation will occur prior to achievement of a sufficient degree of molecular extension for nucleation to be feasible. Thus, both, a minimum strain and strain rate values have to be present for shear flow to induce crystallization. In order to crystallize a polymer melt at a given temperature and shear rate, the shear-induced crystallization effects are found to be critical in relation to the molecular weight (M) [22], a higher M requiring a lower induction time, hence fluid strain. Thus a critical shear strain (at constant shear rate) or a critical shear rate (at a constant shear strain) is a precondition for the effects to occur. The critical shear rate for accelerated crystallization shifts to lower values as molecular weight increases. This is due to underlying molecular relaxation processes.

5.3. Critical orientation molecular weight: model of structure development

Following Keller's observations in elongational flow experiments, we have proposed similar behavior for our shear induced crystallization studies [29]. At a given shear rate, only the molecules having chain length (molecular weight) above a critical chain length (critical orientation molecular weight) can form oriented and stable nuclei. When the polymer melt, containing molecules having broadly distributed chain lengths (molecular weights), is subjected to a shear flow field of a particular $\dot{\gamma}$, only the chains longer than a given critical M^* value will present an extended conformation. However, these molecules will be oriented to different extents. While the degree of chain extension is the ratio of the radius of gyration of the extended chain to that of an unoriented chain, one can compare the radius of gyration in the direction parallel to the deformation field ($R_g^{\parallel}$) with the radius of gyration in the perpendicular direction to the deformation field ($R_g^{\perp}$). In the case that $R_g^{\parallel} \gg R_g^{\perp}$, a large fraction of chains may be oriented, forming many possible primary nuclei, thus accelerating the overall crystallization process. We have considered the final oriented fractions obtained by SAXS, for the different blends to define a low end cut-off at the critical orientation molecular weight M^*. The molecules with molecular weight higher than M^* should be oriented ($R_g^{\parallel} > R_g^{\perp}$), while the rest of the molecules remain unstretched

Table 2
Oriented fractions and critical orientation molecular weight estimated by SAXS and by WAXS

Sample designation	A (%)	Φ^{or}	M^*(SAXS) $\times 10^5$ (g/mol)	X_c^{or}	$M^* \times 10^5$ (g/mol)
I	0	0.18	2.33	0.08	3.29
I/A 96/04	4	0.18	2.38	0.11	3.06
I/A 92/08	8	0.22	2.17	0.11	3.14
I/A 84/16	16	0.29	2.10	0.11	3.47
A	100	0.36	2.70	0.16	5.29

($R_g^{\parallel} = R_g^{\perp}$). The calculated values of the oriented fraction from SAXS in the iPP polymer melt after deformation and subsequent crystallization can be assumed to be proportional to the fraction of the chains in the molecular weight distribution above the critical orientation molecular weight. From GPC chromatograms, and using the calculated final values of the SAXS oriented fraction, the critical orientation molecular weight values corresponding to each sample were determined. The obtained values for the critical orientation molecular weight obtained from SAXS are presented in Table 2. It is noteworthy that with different molecular weight distribution samples, the value of M^* (at 57 s^{-1}) as determined by SAXS is nearly constant. This observation is in support of our assertion that the value of M^* is a critical parameter to characterize relationships between the molecular weight distribution and shear-induced crystallization behavior. We have also used a similar approach to analyze the WAXS data (M^* was determined by the ratio of oriented/unoriented scattering components). We find that the values of M^* determined by WAXS (Table 2) are higher than that by SAXS, but still rather consistent with each other. We again attribute the difference in the M^* values determined by SAXS and WAXS as due to the detection limit (SAXS is about 0.1% crystallinity and WAXS about 1%) and the different nature of the scatterers to be seen. SAXS detects any structures with density contrast, while WAXS detects three-dimensional order in matter. Fig. 11 shows the molecular weight distribution curves obtained from GPC, for the two homopolymers and for the blend I/A 84/16. The edges of the dotted lines indicate the two average limits for M^* obtained. Polymer molecules with molecular weight higher than M^* become oriented whereas chains with molecular weight lower than M^* cannot. Overall, we favor the use of SAXS data to determine the value of M^*, because: (i) the detection limit of SAXS is better than that of WAXS; (ii) the initial SAXS intensity from the quiescent melt is almost negligible. In contrast, the initial WAXS intensity shows a large contribution from the noncrystalline species.

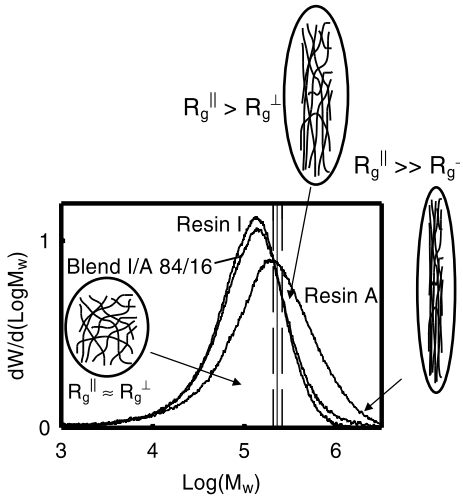

Fig. 11. GPC patterns for resin I, resin A and the blend I/A 84/16. The dotted lines represent the two limits for the critical orientation molecular weight obtained from the SAXS and WAXS oriented fractions of all samples studied.

In summary, we propose a model for the structure development in iPP after a short pulse of high shear in which due to the applied deformation, a gradient of extension in the high molecular weight chains can develop. Molecules with very high molecular weight can be in a significantly extended conformation. As the molecular weight decreases, the chains may be less extended, but still presenting a net orientation, characterized by $R_g^{\parallel} > R_g^{\perp}$. Below a given critical molecular weight orientation, M^*, which apparently depends only on the shearing conditions (not on the MWD), the molecules are not oriented, and give rise to randomly distributed crystallinity This mechanism is depicted over the GPC data in Fig. 11. We acknowledge that the use of SAXS to determine the value of M^* may not be quite accurate as some unoriented lower molecular weight species may be incorporated into the oriented crystals such as in the case of transcrystallization from the nucleating surface in quiescent melts. It is certain that the transcrystalline lamellar structures will be detected as oriented fractions by SAXS. If this is true, then the estimated values for M^* in this work would be, in fact, lower than the real value. However, we feel that such a situation may not take place in flow-induced crystallization. This is because, we believe, the primary mechanism responsible for flow-induced crystallization is through the generation of nuclei instead of large shish or fibrillar structures identifiable by TEM (these structures are not seen in our shear studies). As the dimensions of the nuclei are small, the notion of transcrystallization does not apply. In other words, the "epitaxial growth" from the primary nucleus only results in a single lamella. If the vicinity of the nucleus is occupied by completely unoriented lower molecular weight species, the resulting lamella will quickly lose its original orientation.

We also wish to point out that the M^* value estimated in this study is only valid under the chosen experimental condition (temperature 150°C, shear strain 1428% and shear rate 57 s^{-1}). At the different experimental condition, the M^* value would be very different. For example, the lowering of temperature should significantly reduce the value of M^*, resulting in an increase in orientation of the lower molecular weight species. Thus in practical non-isothermal process such as injection molding, the orientation of low molecular weight species are accessible.

As mentioned earlier, we have observed the presence of a significant contribution of crystallites with β-phase in all our samples. Our studies in progress indicate that, the β-phase crystallites are primarily unoriented, which are located in between the oriented cylindrites with the α- phase. This will be the subject of a future publication.

6. Conclusions

(1) Upon application of a step shear at 1428% strain with a shear rate of 57 s^{-1}, the WAXS patterns of different iPP melts at 150°C show the development of oriented crystallites. Results are consistent with the concept in which long chain iPP molecules are partially oriented and aligned in the flow direction, which enhances (primary) nucleation and causes growth (secondary nucleation) of lamellae perpendicular to the flow direction.

(2) The primary reason for the shear-enhanced crystallization kinetics is due to the generation of primary nuclei, induced by molecular orientation.

(3) A variation in crystallization kinetics after shear with molecular weight distribution is found. The measurements reveal that, the introduction of a very small amount of high molecular weight chains (4%) in iPP of a lower molecular weight, is sufficient to induce drastic changes in the kinetics. This finding indicates that, the long molecules, under shear, are the ones responsible for enhancement of the crystallization kinetics.

(4) In addition to the oriented crystals, unoriented crystals also develop after a step shear. The kinetics of development of these crystals (from WAXS) is similar for all the samples containing even a small portion of the high molecular weight component. The amount of the final unoriented crystallinity is the same for the high molecular weight resins, and for all the blends.

(5) The oriented fractions derived from the SAXS and WAXS patterns allow us to determine the 'critical orientation molecular weight' M^* values. For a given shear rate, M^* is found to be independent of the molecular weight distribution. This finding suggests that, only the polymer molecules having a molecular weight above the 'critical orientation molecular weight' become oriented by shear.

Acknowledgements

We would like to thank Prof. R.S. Stein for helpful discussions. The financial supports for this work has been provided in part by NSF DMR-9732653, US-Spain Science and Technology program 1999 and by ExxonMobil. A grateful acknowledgement is also due to the DGICYT, Spain, grant PB94-0049.

References

[1] Lee O, Kamal MR. Polym Engng Sci 1999;39(2):236.
[2] Bayer RK, Eliah AE, Seferis JC. Polym Engng Rev 1984;4:201.
[3] Ania F, Bayer RK, Tschmel A, Michler HG, Naumann I, Baltá Calleja FJ. J Mater Sci 1996;31:4199.
[4] Rueda DR, Ania F, Baltá Calleja FJ. Polymer 1997;38(9):2027.
[5] Keller A, Kolnaar HWH. In: Meijer HEH, editor. Processing of polymers, vol. 18. 1997. p. 189–268. (chap. 4).
[6] Pople JA, Mitchell GR, Sutton SJ, Vaughan AS, Chai CK. Polymer 1999;40:2769.
[7] Haas TW, Maxwell B. Polym Engng Sci 1969;9:225.
[8] Kobayashi K, Nagasawa J. J Macromol Sci, Phys B 1970;4(2):331.
[9] Wereta A, Gogos C. Polym Engng Sci 1971;11:19.
[10] Krueger D, Yeh GSY. J Appl Phys 1972;43:4339.
[11] Fritzsche AK, Price FP. Polym Engng Sci 1974;14:401.
[12] Tan V, Gogos C. Polym Engng Sci 1971;11:512.
[13] Lagasse RR, Maxwell B. Polym Engng Sci 1976;16:189.
[14] Fritzsche AK, Price FP, Ulrich RD. Polym Engng Sci 1976;16:182.
[15] Monasse B. J Mater Sci 1995;30:5002.
[16] Sherwood C, Price F, Stein R. J Polym Sci (Polym Symp) 1978;63:77.
[17] Vleeshouwers S, Meijer HEH. Rheol Acta 1996;35:391.
[18] Tribout C, Monasse B. Haudin. Colloid Polym Sci 1996;274:197.
[19] Varga J. J Mater Sci 1992;27:2557.
[20] Varga J, Karger-Kocsis J. J Polym Sci, Part B, Polym Phys 1996;34(4):657.
[21] Kargin VA, Andrianova GP. Dokl Akad Nauk USSR 1962;146:1337.
[22] Binsbergen FL. Nature 1966;211:516.
[23] Kumaraswamy G, Issaian AM, Kornfield JA. Macromolecules 1999;32(22):7537.
[24] Kumaraswamy G, Varma RK, Issaian AM, Kornfield JA, Yeh F, Hsiao BS. Polymer 2000;41(25):8931.
[25] Misra S, Lu FM, Spruiell JE, Richeson GC. J Appl Polym Sci 1995;56:1761.
[26] Moitzi J, Skalicky P. Polymer 1993;34(15):3168.
[27] Haudin FJ, Monasse B. J Mater Sci 1999;34:2089.
[28] Eder G, Janeschitz-Kriegl H, Liedauer S, Schausberger A, Stadlbauer W, Schindlauer G. J Rheol 1989;33:805.
[29] Somani R, Nogales A, Hsiao B, Srinivas S, Tsou AH, Sics I, Ezquerra TA, Baltá Calleja FJ. Macromolecules 2000;33(25):9385.
[30] Hongladarom K, Ugaz VM, Cinader DK, Burghardt WR, Quintana JP, Hsiao BS, Dadmun MD, Hamilton WA, Butler PD. Macromolecules 1996;29:5346.
[31] Ran S, Zong X, Fang D, Hsiao B, Chu B, Ross R. J Appl Crystallogr 2000;33:1031.
[32] Dean DM, Rebenfeld L, Register RA, Hsiao BS. J Mater Sci 1998;33:1.
[33] Samuels RJ, Yee RY. J Polym Sci, Part A2 1972;10:385.
[34] Padden FJ, Keith HD. J Appl Phys 1966;37:4013.
[35] Lotz B, Wittmann JC, Lovinger AJ. Polymer 1996;37:4979.
[36] Lotz B, Graff S, Wittmann JC. J Polym Sci, Part B: Polym Phys 1986;24:2017.
[37] Wang ZG, Hsiao BS, Sirota EB, Agarwal P, Srinivas S. Macromolecules 2000;33:978.
[38] Wunderlich B. Macromolecular physics, 2. London: Academic Press, 1976 (chap. 6).